APPLICATION OF EVOLUTIONARY OPTIMIZATION ALGORITHMS IN COMPUTATIONAL OPTICS

Daniel Erni[1,2], Dorothea Wiesmann[1,3], Michael Spühler[1,2], Stephan Hunziker[1,2], Esteban Moreno[1,2], Benedikt Oswald[2], Jürg Fröhlich[4] and Christian Hafner[2]

[1]*Optical Signal Processing Group* of the
[2]Laboratory for Electromagnetic Fields and Microwave Electronics,
and the [3]Electronics Laboratory,
Swiss Federal Institute of Technology, ETH-Zentrum,
Gloriastrasse 35, CH-8092 Zürich,
[4]Institute for Operartions Research, University of Zürich
Moussonstrasse 15, CH-8044 Zürich
contacts: erni@ifh.ee.ethz.ch

ABSTRACT – The spatial and spectral treatment of electromagnetic fields express an essential operation regarding, e.g., the functionality of dense integrated optical devices. Such molding of fields can hardly be handled without sophisticated heuristic optimization tools. By means of five design examples we have demonstrated that evolutionary algorithms (EA) are highly qualified to solve "real world" inverse problems considering various applications in the field of planar integrated optics, optical communication technology, and dielectric material modeling as well. In comparison to other optimization schemes EAs are even able to deliver structural and temporal information of the device under optimization which is an important feature when targeting computer guided engineering and virtual design platforms.

1. INTRODUCTION

Evolutionary algorithms (*EA*) [1] are computer codes which emulate the search process of natural evolution. This class of optimization algorithms rests upon the collective learning process within a population of individuals, each of which represents a search point in the space of potential solutions to the given problem. Because of an implicit parallelism in the search behavior they avoid the common pitfalls of local optimization algorithms, but hold the promise of finding novel solutions perhaps not thought to exist.

The latter aspect – i.e., the structural optimization feature – has successfully been applied to several different types of design problems in planar integrated optics [2], such as single longitudinal mode multi-cavity laser diodes [3], [5]-[10], ultra-short non-periodic segmented spot-size converters for highly efficient chip-to-fiber coupling [9]-[13] and concatenated Bragg gratings for apodized add/drop filters in wavelength division multiplexing (*WDM*) network nodes [14]. In earlier contributions [15], [16], *evolutionary algorithms* have also been considered as very efficient regarding their *parameter estimation* features in the context of speeding up costly computational electromagnetics simulations. They have also been applied when optimizing frequency channel distributions in fiber optic *SCM*-links [17] and for the determination of analytical dispersion models for complex and highly lossy dielectric materials [18].

In the paper presented here, we will outline all design examples mentioned above. Therefore, the remainder of the paper is organized as follows: In Section 2, we briefly explain our special type of *evolutionary algorithm* which is then used for the optimization of an active waveguide device namely a non-periodic coupled-cavity semiconductor laser diode. Section 3 is dedicated to the design of realistic apodized concatenated Bragg gratings as highly selective add/drop filters for wavelength division multiplexing (*WDM*) applications. The spatial treatment of guided modes by a non-periodically segmented waveguide structure leading to a very compact and efficient spot-size converter is reported in Section 4. Section 5 describes the optimization of frequency channel distributions in fiber optic *SCM*-links and the determination of an analytical dielectric material model is given in Section 6.

After these elucidations, a brief outlook is given, focusing on some algorithmic prospects (Section 7) and tracing two aspects towards computer guided engineering (Section 8) as well. We conclude our contribution with a short summary in Section 9.

2. MULTI-CAVITY LASER TOPOLOGIES

An economically priced monolithic GaAs/AlGaAs laser diode with an emission wavelength around *852 nm* represents an attractive light source for low-cost high-precision time and distance metrology. Such single-longitudinal-mode laser operation usually relies on distributed Bragg reflector (*DBR*) laser topologies or distributed feedback (*DFB*) lasers respectively. Both utilize a fine-scale grating mostly having periods on the orders of a few hundred nanometers. This puts high demands even on the state-of-the-art lithographic reproduction, resulting in very high costs.

In order to focus on simple laser processing, we restrict our design to large-scale non-periodic perturbations in the form of multi-section cavity structures. Such irregular topologies are now to be optimized with respect to given laser specifications.

The type of *breeder genetic algorithm* (see also [4]) presented here works on fixed-length bit-strings. It starts by initializing a population of $N = 50$ bit-strings randomly. Then the population evolves by using probabilistic *genetic operators* for reproduction purposes. Within this frame, two parent-strings are selected by the *fitness*-proportional *roulette-wheel selection* process. Two off-spring are then generated using *two-point crossover* and *mutation*. Referring to the forward problem a laser simulator is activated, delivering all characteristic data needed for the quality rating of each off-spring. After judging the quality (*fitness*) of these new individual two advantageous aspects of our implementation should be mentioned [5], [6]: *1.)* every new individual is checked whether it is already included in the population. Allowing no duplicates guarantees a certain diversity and avoids premature convergence. *2.)* only better individuals than the worst enclosed in the population are inserted, e.g., a *strict breeding* is done. The whole reproduction process defines a loop which is carried out until the number of calculated individuals reaches a certain predefined value.

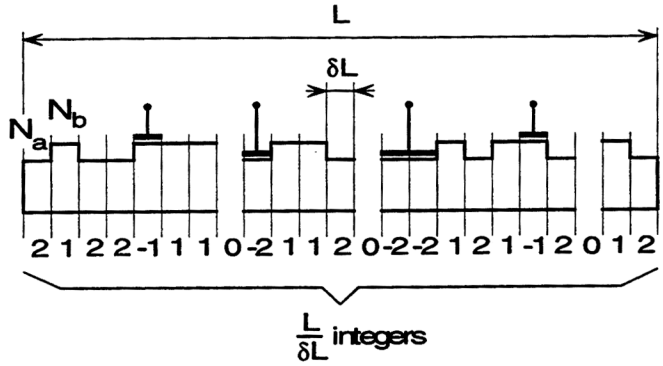

Fig.1: Representation of the non-periodic multi-cavity laser structure (phenotyp) by a 5-valued integer string (genotyp) including contact electrodes for current injection.

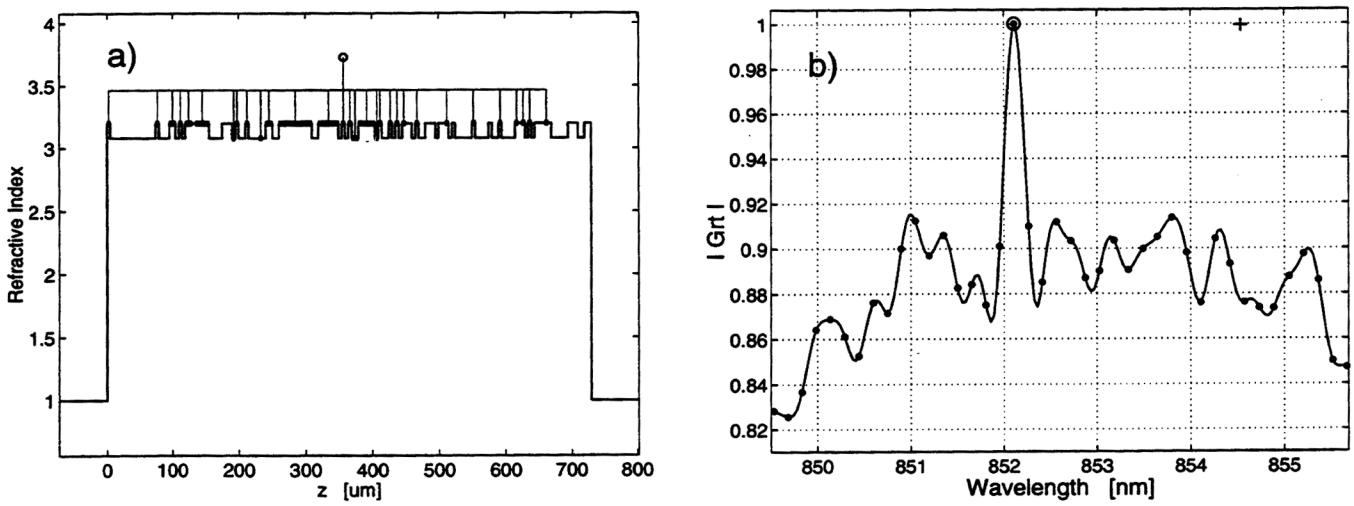

Fig.2: Best performing laser solution. a) The effective refractive index distribution along the cavity shows 59 sections at a total length of 730 μm. The position of current injection is sketched by its corresponding electrode (labeled as a bold line). b) Corresponding round-trip gain spectrum G_{rt}. Lasing occurs at the circle, all round-trip phase zeros are marked with dots and the small cross indicates the material gain maximum. The distinct mode selectivity should be considered in the context of the very low effective refractive index contrast of the perturbed laser cavity.

In order to judge the quality of each search point a *fitness* value has to be defined, relying on the forward solver's specific output. As the main validation criterion within all further simulations the round-trip gain G_{rt} is taken in terms of a potential mode-selectivity at lasing threshold. The round-trip gain G_{rt} represents the oscillation condition itself. According to our laser structure, the overall *fitness* is defined as a sum of three different *fitness* numbers: one concerns the side-mode suppression within the round-trip gain spectrum. A second term validates the coincidence between the position of the material gain peak and the specified wavelength of *852 nm*. The third term measures the wavelength-difference between the lasing point and this specification.

Following [8], a *representation scheme* (*Fig.1*) of the multi-cavity laser structures is obtained using a fine-scale discretization. Assuming a maximal laser length of $L = 1000\ \mu m$ and a discretization's resolution of $\delta L = 5\ \mu m$, the laser topology can be described as an array with $L/\delta L = 200$ integers each representing one segment within the potential laser cavity. Each segment having an effective refractive index N_a or N_b is assigned to an integer value of *2* or *1* respectively. A *"don't care"* represented by an integer value of *0* does not influence the decoding operation when mapping the integer array (*genotype*) into its corresponding physical representation (*phenotype*).

In combination with genetic operators such as *crossover* and *mutation* the optimization procedure has the ability to build up lasers with different lengths. Further we allow the optimizer to *"decide"* how the current injection into the laser structure has to be performed when searching for appropriate numbers and positions of contact electrodes. A contacted segment may simply be marked by a reversed sign of its corresponding integer (*allele*) leading to a 5-valued *genotype* and therefore to a tremendous large search space of $200^5 \approx 10^{140}$ search points.

The performance of the multi-cavity laser structure is evaluated by applying the well known transfer-matrix analysis [19]. All material properties involved such as material gain and the carrier induced refractive index change are obtained from optical gain measurements and are implemented as an appropriate spectral model [5]. The effective refractive index difference representing the perturbation is assumed $1.92 \cdot 10^{-2}$.

Our optimization scenario [8] after *33'720* evaluated individuals yields a maximal performing structure (*Fig.2a*) with a *fitness* of $1.056875 \cdot 10^6$. The spread of *fitness* values within the optimized population is around *4%*. It should be noted that good solutions ($fitness > 4 \cdot 10^5$) are already achieved after less than *700* iterations. The round-trip gain spectrum G_{rt} of the best performing laser structure (*Fig.2b*) shows the desired distinct wavelength selectivity permitting single longitudinal mode lasing operation at *852.10 nm*. Here the current injection reaches a threshold value of *11.98 mA* when lasing.

3. CONCATENATED GRATING FILTERS

Wavelength division multiplexing (*WDM*) at wavelengths of *1520-1570 nm* in optical fiber networks for, e.g., *2.488 Gb/s* data rates demands (integrated) optical filters for adding and dropping single wavelength channels at certain network nodes. Bragg grating based filters become very attractive, when the requirements for intra-channel crosstalk are stringent. Unfortunately, uniform Bragg gratings suffer from poor sidelobe suppression in their spectral response. If only a certain inter-channel crosstalk, i.e. a certain sidelobe level at the neighboring channel, is allowed the high sidelobe results in a large channel spacing and thus in a small bandwidth utilization. In order to circumvent this deterioration apodized grating structures – i.e., gratings with longitudinally varying mode coupling constants according to a bell-like weighting function – are strongly recommended.

An obvious way to alter the coupling strength of surface corrugated gratings consists of a correspond-

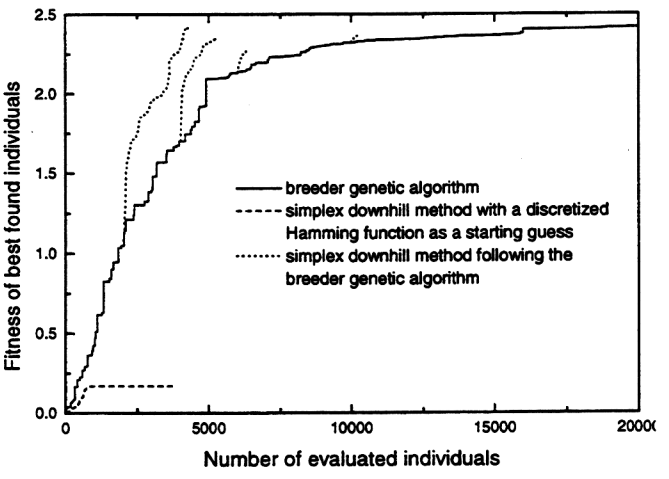

Fig.3: Fitness evolution of different grating filter optimization attempts as a function of evaluated individuals. A discrete valued Hamming distribution of the coupling constant acts here as a starting guess for the initial SDH.

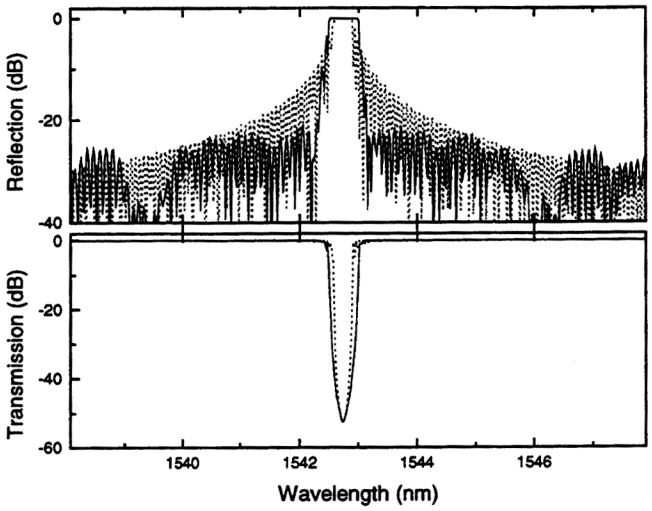

Fig.4: Simulated spectral response of a concatenated grating (solid line) and of the equivalent uniform grating (dotted line). Both gratings are 11 mm long.

ing change in etch depth of the periodic ridge waveguide corrugation (another attempt using a direct UV-writing technology [20], [21] to locally change the planar glass waveguide's effective refractive index is still under investigation). However, to preserve process reproducibility a binary grating, e.g., a constant etch depth is preferred. One apodization method obeying this constraint exploits the dependence of the coupling coefficient on the grating duty cycle [22]. In this approach the minimum coupling coefficient is

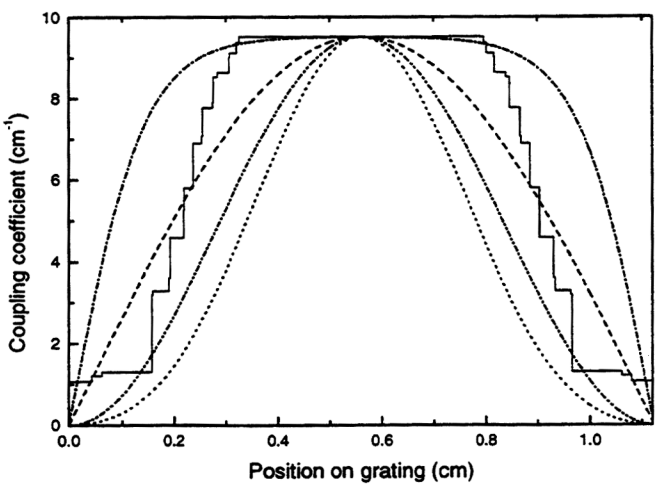

Fig.5: Coupling strength distribution along the grating for the optimized concatenated grating (solid line) and several conventional taper functions (Blackman function (dotted line), raised sine (dash-double dotted line), sine (dashed line), positive hyperbolic-tangent profile (dash-dotted line)).

determined by the most extreme duty cycle that is producible, i.e., the one deviating most from *50%*, which has to be found experimentally. We found a minimum duty cycle of about 10% to be a typically achievable value for glass waveguides with grating periods of about *500 nm* [14]. In consequence, any apodization function realized within our production technology will be truncated. Classical windowing functions of, e.g., a Hamming (or a raised cosine) shape, suppress all sidelobes below a certain level (e.g. *–50 dB*) that is given by the function itself and the accurateness of its practical realization. Thus, all classical windowing schemes tend to perform unsatisfactory when truncated (for the Hamming window the sidelobe level raise up to *–14 dB* when this apodization function has to comlpy with a minimal available duty-cycle of 10%). We have therefore decided to look for apodization functions that are optimized, taking experimental constraints into account with the more pragmatic goal to just suppress all sidelobes outside a certain bandwidth.

The choice of the optimization scheme was also influenced by the discrete nature of the actual problem representation: the gratings are usually implemented by a vector scan electron beam lithography system with a discrete address grid. The set of producible duty cycles and hence the set of realistic coupling coefficients is thus given once the writing field size has been chosen. The only parameters that are available when optimizing the coupling strength profile are the lengths of the different grating regions. Furthermore, each length should be an integer multiple of its corresponding grating period. Therefore, finding an appropriate apodization scheme – i.e., to trace an appropriate concatenation of different subgratings – always represents a crucial combinatorial optimization problem which is efficiently solved only by a *genetic algorithm* [5], [6], [8].

To evaluate the gratings we first have to define the desired crosstalk levels, e.g., an intra-channel crosstalk better than *-30 dB* within a bandwidth of *0.4 nm* and an inter-channel crosstalk of *-25 dB* outside a bandwidth of *0.8 nm*. According to [23] the inter-channel crosstalk requirements for neighboring channels is less strict and amounts to *–20 dB*. We use the larger value to give the optimizer a larger margin. In each iteration step the grating response is calculated using the well known transfer-matrix method [24]. According to the given filter specification, the overall *fitness* is consequently defined as a sum of two different fitness constituents: One number validates the actual spectral filter response with respect to the desired inter-channel crosstalk and a second term measures the spectral deviation with regard

to the given intra-channel crosstalk specifications. *Fig.3* shows the fitness evolution for a grating consisting of *40* grating sections with corresponding duty cycles. In order to compare our *breeder genetic algorithm* (solid line) with alternative optimization schemes we have also plotted the evolution when enabling a specific *simplex downhill* (*SDH*) optimization working on discrete number spaces (dotted line). As starting guess for the coupling strength distribution we used a discrete valued Hamming function. Referring to the corresponding trace in *Fig.3* it is clearly visible that the *simplex downhill* method gets caught in a local optimum. Additionally, we have stopped our *genetic algorithm* after a certain number of evaluated individuals and have it followed by a *simplex downhill* optimization (several dashed lines). The *simplex downhill* usually tends to accelerate the down tracking of promising parameter sets nearby a fitness landscape's local optimum. But it is noteworthy to realize that a prior global optimization procedure is always mandatory.

After *2000* iterations (and additional *1300 down hill simplex* iterations) a representative design has led to *50* grating solutions where the best performing one has a potential bandwidth-utilization-factor of *50%* at an intra-channel crosstalk of *-30 dB* and an inter-channel cross-talk of *-21 dB* close to the Bragg resonance which complies well with the requirements (*Fig.4*).

As shown in *Fig.5* the *3 μm* wide ridge waveguide Bragg gratings consist of *40* different subgrating sections having an overall length of *11 mm*. All of them are producible in an inexpensive planar *SiO_2/SiON* glass technology with an available etch depth of *100 nm*. Comparing our design approach to, e.g., commonly used thin-film interference filter synthesis methods [25], our *evolutionary optimization* procedure potentially reveals an objectionable computational effort. But from the viewpoint of a *realistic* design, this sobering prospect should be reassessed into a promising one especially with regard to our design procedure's feasibility while including all critical nonidealities of the technological production process.

4. ULTRA SHORT SPOT-SIZE CONVERTER

In the last two sections we described how our *evolutionary algorithm* can be used to comply with the *spectral* specifications within a design procedure of integrated optical devices. The example being now under consideration is dedicated to the *spatial* treatment of optical fields regarding the functionality of such devices. Because of its large refractive index difference ($\delta n \approx 0.02$) the planar *SiO_2/SiON* glass waveguide technology has the

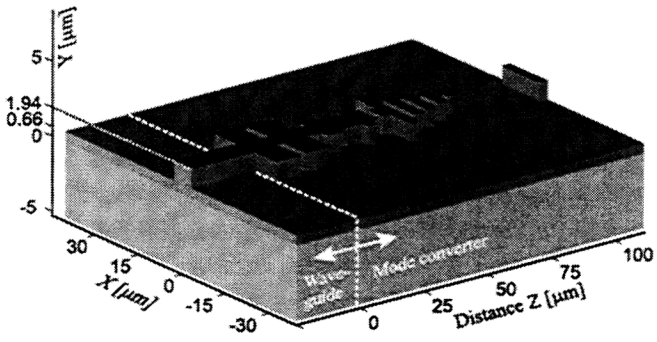

Fig.6: Example of a planar spot-size converter. For visualization purposes the upper cladding is not shown. Only changes in the width and segmentation are supported. Such structures can be manufactured as simply as a normal waveguide.

benefit of allowing small bending radii on the order of *1 mm*. Therefore, this inexpensive technology meets the requirements for dense integrated optics. But such strong waveguiding has inevitably its drawback considering the mode mismatch at an optical transition between chip and single mode fiber. Direct butt-coupling would cause losses of more than *3.5 dB*. In order to reduce these losses, the modal shape of the integrated waveguide's fundamental mode has to be converted into a shape as close as possible to the fundamental fiber mode.

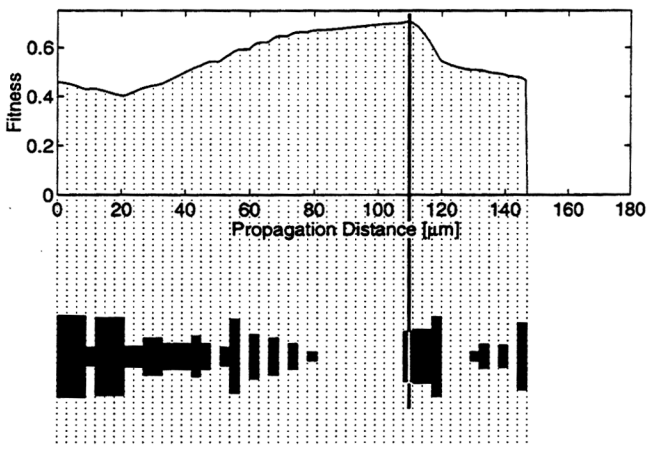

Fig.7: The fitness evolution through the converter is shown here. The real structure will be cut at the position where the highest fitness is obtained. Therefore the implemented converter is usually considerably shorter than the total structure. The fitness is calculated after each BPM propagation step. The best fitness ever encountered (here at about 110μm, shown by the vertical line) is retained as the overall fitness of the converter.

5. FREQUENCY CARRIER DISTRIBUTION

Today, fiber optic links are substantial parts of modern communication systems [28]. It is therefore important to know their distortion and noise properties [29]. Systems with subcarrier multiplexing (*SCM*), in which often equally spaced *rf* carriers with different amplitudes lie within a narrow band, have very low intermodulation-distortion (*IM*) specifications, as do common antenna television systems (*CATV*). In optical transmission links with standard fibers and directly intensity-modulated lasers at *1.3 μm*, the main contribution to the distortion is due to mixed – static and dynamic – laser nonlinearity [30]. In such communication systems only odd orders of the nonlinearity have to be considered when a weak nonlinearity is assumed.

It is rather the resulting 3^{rd} order *IM* which is of technical relevance [31]. Having, e.g., a transmission band of $f_1,\ldots,f_n$ equally spaced *rf* carrier frequency channels, where M_C is assumed to be the set of operational carrier indices, then 3^{rd} order IM generates mixing products of the following kind: $f_i+f_k-f_\ell$, $f_i-f_k+f_\ell$, $-f_i+f_k+f_\ell$, $\forall\ i, k, \ell \in M_C$. All mixing products which coincide with a frequency f_r within the transmission band obey $i+k-\ell = r$ or $i-k+\ell = r$ or $-i+k+\ell = r$, $\forall\ i, k, \ell \in M_C$.

In order to propose M_C as an optimal carrier distribution, one has to look for operational *rf* carrier frequencies within the transmission band whose *IM* products do minimally interfere amongst themselves as well as with their engendering carriers, respectively.

In an ideal case, where one simply wants to prevent a carrier to overlap with those *IM* products stemming from the remaining ones, all distances between pairs of carrier frequencies should be different like $i-\ell \neq r-k$. A set M_C with such properties is also called *"Golomb ruler"* [17] when containing *0* as an additional element. Therefore, placing N operational carriers within a minimal transmission bandwidth of $n > N$ channels, means nothing else than looking for a preferably short *Golomb ruler* whose largest element should be as small as possible.

Computational solutions are only available for $n >> 16 \geq N$. Thus, considering dense carrier distributions inevitably leads to a combinatorial optimization procedure, where a minimal intermodulation-to-carrier-ratio (*IM/C*) should be aspired for occupied

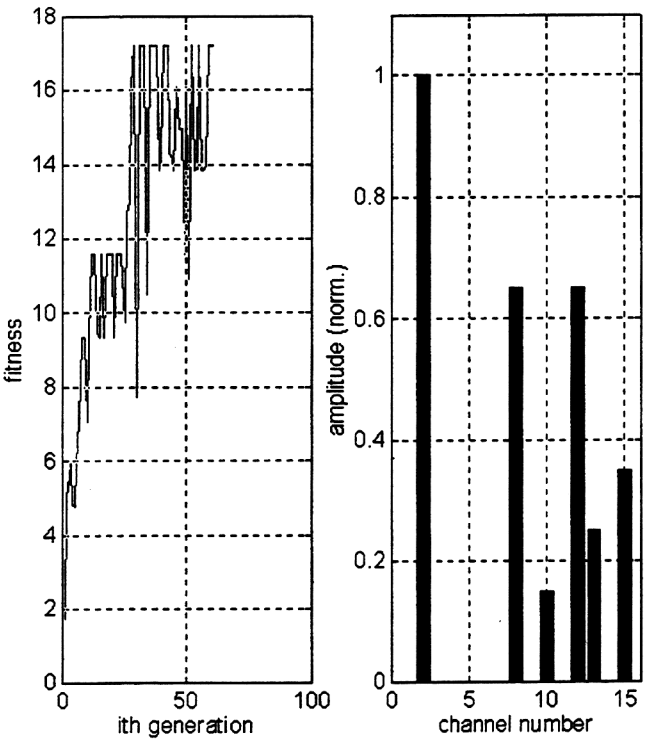

Fig.9: Optimal distribution of 6 different carriers within 15 equally spaced transmission frequency channels. (Left) fitness evolution during optimization, (right) transmission band with optimally placed carriers (shown as bars).

channels as well. The optimization task becomes even more severe when taking into account different carrier amplitudes. There are

$$M_1 = \binom{n}{N}$$

combinations of how to distribute N operational carriers within n transmission channels. Assuming a given set of N different amplitudes within each distribution pattern additional $M_2 = N!$ permutations of carrier amplitudes have to be taken into account. As *genotype* of a particular carrier distribution, we define a bit-string representation for a pair of ordinal numbers (m_1, m_2) $\forall\ m_1 \in [1, M_1]$, $m_2 \in [1, M_2]$, where the first of them addresses the combination state of the particular pattern and the second characterizes its permutation state respectively. The *fitness* of a particular pattern is then calculated with respect to the worst *IM/C* of all occupied transmission channels involved.

Our exemplary *evolutionary optimization* problem [17] includes a set of *6* given carrier amplitudes to be placed within a transmission band of *15* equally spaced frequency channels. As optimizer we use a standard *genetic algorithm* (generation based *genetic algorithm*: traditional *one-point crossover, 60% selection probability, 1% mutation rate*) which operates on a population size of *300* individuals. A best performing solution was found after *30* of totally *60* generations. *Fig.9* shows the optimal carrier distribution leading to a minimal 3^{rd} order *IM* distortion of the fiber optic *SCM*-link.

The optimization problem presented here is also of prime importance regarding the design of very advanced optical *WDM*-systems. For high-speed *WDM*-systems the simultaneous requirements of high launched power and vanishing fiber dispersion lead to the generation of new optical frequencies by four-photon mixing. These generated waves can interfere with system operation while degrading the system capacity by intermodulation distortion and additional noise generation in band limited erbium doped fiber amplifiers (*EDFAs*). In order to prevent phase matching of these waves one is tempted to allow a small amount of fiber dispersion at an additional expense of system capacity [32]. Hence, an optimization of optical carrier distribution enables the reduction of intermodulation distortion without need of any dispersive fiber.

6. DIELECTRIC MATERIAL MODELS

In this section, we report an *evolutionary optimization* based method for the determination of the dispersive dielectric properties $\underline{\varepsilon}_r(f)$ of natural materials exhibiting high dielectric and ohmic losses over a wide frequency range. Accurate information on the dependence of dielectric properties of (mixtures of) natural materials on content of, e.g., water or hydrocarbons, and also on temperature is of considerable importance in a number of applications, e.g., in environmental engineering, geophysics, mathematical geology and chemical process engineering. The microstructure of such multiphase mixtures are generalized by a structural material matrix representing the characteristic distribution of its constituents. This concept of *structural units* [33] – which is a picture for capturing the microstructural and compositional information of the randomly distributed constituents within a dielectric host material – becomes particularly attractive when linked to an accurate spectral dispersion

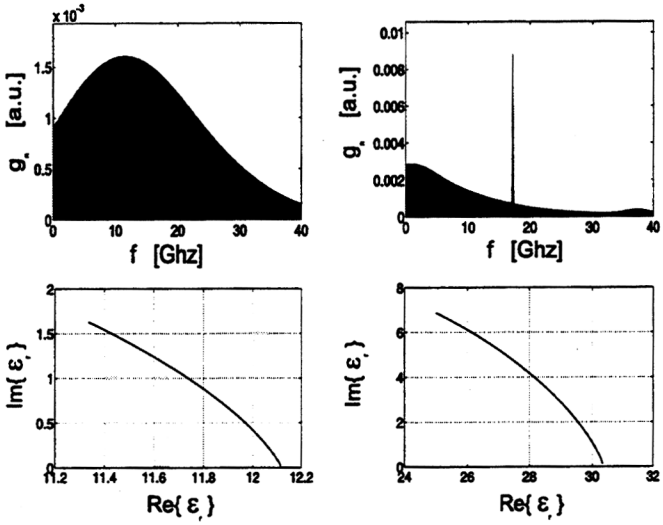

Fig.10: (Top) relaxation spectra $g_n(f_r^n)$ and (bottom) Cole-Cole plot of $\underline{\varepsilon}_r(f)$ for a volumetric water content of (left) $\Theta = 0$, and (right) $\Theta = 15\%$ where the relaxation frequency of free water is clearly reproduced by the proposed model. The frequency range of the measured scattering data is $f = 10$ MHz...3 Ghz.

model in an effective medium approach. Hence, disposing of such an accurate macroscopic description of dielectric mixtures could even have a seminal impact on advanced topics in physical optics such as wave localization phenomena due to random scattering, photon diffusion, coherent backscattering and has yet led to the *diffusive wave spectroscopy* as a new optical measurement technique in material science and food engineering [33].

The analytical material model presented here is extracted from electromagnetic scattering data of a corresponding coaxial transmission line measurement setup. Following the classical *Debye* model for the relative permittivity we propose a weighted linear superposition of *N* different *Debye* models

$$\underline{\varepsilon}_r(f) = \varepsilon_\infty + (\varepsilon_s - \varepsilon_\infty) \cdot \sum_{n=1}^{N} \frac{g_n(f_r^n)}{1 + i\left(\frac{f}{f_r^n}\right)} - i\frac{\sigma_{diel}}{2\pi\varepsilon_0 f}$$

where ε_s stands for the static limit, ε_∞ for the high frequency limit, ε_0 describes the vacuum permittivity, σ_{diel} accounts for the ohmic conductivity of the material involved, f_r^n represents the relaxation frequency of the *n*-th *Debye* model and $g_n(f_r^n)$ defines a normalized relaxation weighting function which on itself is composed by a finite set of *G* different *Gaussian* relaxation functions. Choosing such a finite base of the relaxation

spectra $g_n(.)$ mainly helps to circumvent the *ill-posedness* of the model estimation problem. The *genotype* consists of an appropriate binary representation of all parameter values to be optimized. The parameters include the weightings, the relaxation frequencies and bandwidths of the numerous *Gaussian* relaxation components, the conductivity σ_{diel} and both limits, ε_s and ε_∞ of the permittivity model. We can define the *fitness* of a potential solution as the quality of the approximation of calculated and measured scattering spectrum respectively. Referring to the matching of the scattering phase between analytical model and measured data the resulting *fitness* function behaves like a jagged multimodal landscape provoking serious pitfalls for commonly used optimization algorithms.

As an *evolutionary* optimized example we present the analytical description of *Bentonite*, a highly lossy, very complex clay like material with and without volumetric water content Θ [18] at a temperature of *23°C*. The behavior of our estimated model is shown in *Fig.10*, whereas the corresponding parameters can be obtained from the following table *Tab.1*.

	$\Theta = 0$	$\Theta = 15\%$
# individual	*21'373*	*21'552*
ε_s [–]	*12.1236*	*30.4155*
ε_∞ [–]	*3.00012*	*2.18958*
σ_{diel} [*mS*]	*18.314*	*99.9847*

Tab.1: Optimized parameter set for Bentonite at two different humidity states.

To conclude we derived a very general analytical material model for complex and highly lossy dielectric materials which outperforms commonly used *Debye* models in terms of flexibility and accuracy as well. Our approach is able to cover different distinct relaxation phenomena which are not easily tractable within a straight forward *ab initio* dispersion formula.

7. PROBLEM-BASED ALGORITHMIC PROSPECTS

We have demonstrated *evolutionary algorithm's* applicability to various optimization problems within the field of computational optics and electromagnetics. After all, this is because most of such real-world problems could easily be transformed into combinatorial problems as well, where *evolutionary algorithms* and especially *genetic algorithms* are claimed to belong to the best suited ones compared to other heuristic optimization codes. In addition, this kind of optimization scheme delivers much more general information about what actually leads to a good solution. Therefore, it permits us to implement superior meta-optimization strategies which rely on, e.g., a population based *information gathering*. Such an *information gathering* procedure includes *structural information* concerning typical patterns [8] within optimized individuals as well as *temporal information* [11] of the evolution process itself. In the following, both types of *information gathering* will be elucidated in the context of a corresponding application.

7.1 STRUCTURAL INFORMATION PROCESSING IN THE CONTEXT OF MULTI-CAVITY LASER DIODE OPTIMIZATIONS

All optimization scenarios presented in Section 2 appear to converge to an optimal laser structure and it seems that not even a continuation of the optimization process up to some higher iteration number enables the generation of better performing individuals. In addition, most of the statistically available information concerning a "final" state of a population's evolution (e.g., the decreasing spread of fitness values) usually lacks in reproducing the optimizer's potential for a further improvement.

Therefore a structural analysis of all individuals, i.e., searching for frequent and successful patterns within this optimized population could probably answer two questions: First, is such an *information gathering* procedure capable of delivering a novel population whose prospects look more promising within a further optimization attempt? Second, is it also possible to formally acquire insight as to what actually leads to well performing laser structures?

The *information gathering* based on pattern analysis [8] is simply done by evaluating the frequency of appearance of characteristic Q bit-pattern ($Q < L/\delta L$) within the population. By stepping a Q bit wide window along each individual's genotype a corresponding number of different Q bit-strings can be extracted. All these strings are then sorted according to their pattern label, thus assigning each pattern to its frequency of appearance (*Fig 11b*). A similar procedure delivers the

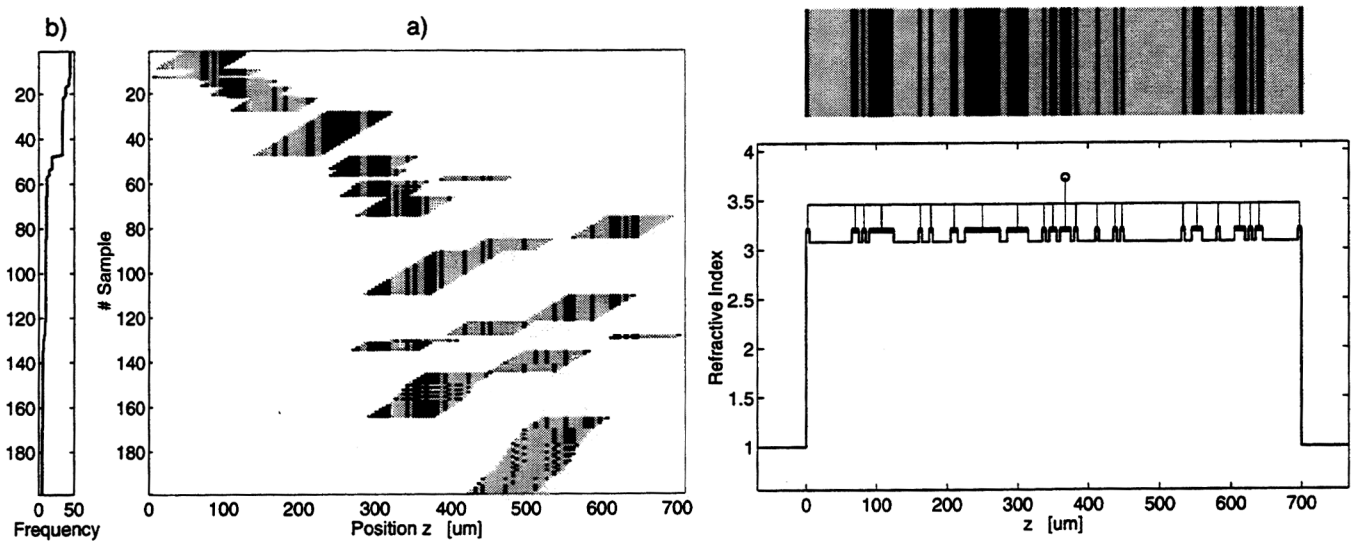

Fig.11: Pattern analysis considering the final population of the optimization scenario described in Section 2: a) Distribution of characteristic 18-bit-patterns along the laser structure and ranked by its frequency of appearance. b) Corresponding frequency of appearance of these patterns. For visualization purposes the pattern analysis has been restricted only to the high and low refractive index segments of the decoded cavity structure (left). Typical cavity refractive index pattern deduced from the 18-bit-pattern distribution (top right). The corresponding non-periodic coupled cavity laser structure (bottom right) consists of 45 sections and has a total length of 700 μm.

most frequent position for every Q bit-pattern within this ranking, leading to the distribution scheme shown in *Fig.11a*). Finally, the distribution of characteristic Q bit-patterns enables us to deduce a typical laser structure which is believed to gather all the specific information needed to qualify as a good solution. The typical laser structure of *Fig.11* is obtained by counting each specific allele value of all pattern sequences at the considered segment position. The counting procedure itself employs a weighting which is proportional to the pattern's frequency of appearance. Therefore, the most frequent parts of patterns will always obtain recognition. Choosing pattern lengths between $Q = 3$ bit and $Q = 90$ bit up to *88* different typical laser structures can be obtained contributing partly to a novel starting population for a further optimization.

In order to validate a population's diversity D a particular non-binary definition of the Hamming-distance [6] has to be specified. We therefore investigate the distribution $\delta D(m)$

$$\delta D(m) = \frac{2}{N \cdot (N-1)} \cdot \sum_{i=1}^{N-1} \sum_{j=i+1}^{N} \rho_H\left(\vec{b}_i(m), \vec{b}_j(m)\right)$$

which measures the average number of appearance of incongruous alleles at the m-th genotype position considering all N integer strings of the population, whereas ρ_H values the incongruity between string $\vec{b}_i$ and $\vec{b}_j$ at position m. The summation of $\delta D(m)$ over the total string length immediately yields the diversity D mentioned above.

Within the optimization scenario presented in Section 2 different population stages have been analyzed according to the appearance of common patterns. As an example, the *information gathering* procedure has yielded 15 typical laser structures, forming a novel population, with some individuals performing even better, and whose diversity is around *13* bit. This represents a distinct increase compared to the *8* bit of the considered underlying population. Further details of the re-optimization process including such typical laser structures are elaborated in [8].

Coming back to the typical laser structure shown in *Fig.11* it can be noted that especially the regions neighboring the two laser facets are strongly correlated and imply a certain robustness against optimization interferences. Thus, changing segments from inner regions of the cavity has proved as a more successful policy while tracking down well performing laser topologies. This assumption is clearly confirmed when investigating the distribution $\delta D(m)$. Inspecting the configuration shown in *Fig 12*

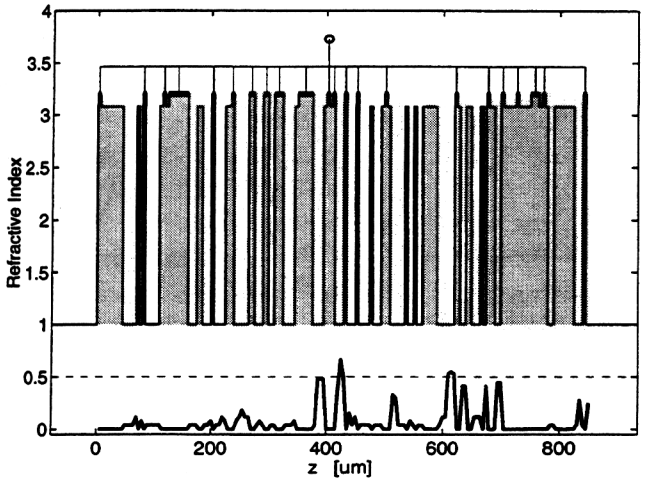

Fig.12: Diversity distribution δD (bold line) mapped along a corresponding decoded cavity configuration considering all genotypes of the underlying final population i.e. of the optimization scenario. The shaded sections indicate locations, where the congruence of all genotypes tends to be exact and the optimizer's interference is therefore believed to be negligible whereas the gaps stand for the position of distinct incongruity within the genotypes involved. The summation of δD over the total string length z immediately yields the diversity D.

one may be tempted to allocate the shaded regions to resistant characteristic patterns. But, because of its different algorithmic background neither the structure given by the shaded regions in *Fig.12* nor the typical cavity topology of *Fig.11* are rigorously comparable to each other. The typical cavity topology is generated when gathering the common pattern information within a population whereas the structure given in *Fig.12* puts the focus on all its differences.

In conclusion, our characteristic pattern analysis reveals a noteworthy feature: Nearly independent of the state of a population's convergence the proposed *information gathering* procedure delivers mostly one individual whose fitness exceeds that of the best performing structure of the underlying population. Therefore we suggest our *information gathering* be used as a sort of meta-optimization strategy. Increasing a population's diversity without degrading the corresponding fitness could be regarded as a useful mean to *revitalize* a population's prospect when looking forward to a further optimization attempt [8].

7.2 TEMPORAL EVOLUTION ASPECTS IN THE SPOT-SIZE CONVERTER DESIGN

Our evolutionary optimization scenario presented in Section 4 also delivers *temporal information* which may be reassessed in the framework of a superior solution strategy. One of the main differences between classical heuristic optimization procedures such as, e.g., *Monte Carlo* or simple *hill-climbing* methods and evolutionary optimization procedures is their implicit parallel search mechanism. As it is demonstrated later, any successful converter contains characteristic substructures that significantly contribute to good performance. In our procedure it is possible to keep track of such substructures during evolution. In order to obtain the corresponding data of the traces, substructures of 10 segments length were compared using a sort of relaxed structural correlation scheme: If no more than 3 segments of that substructure differ from one individual to another, both individuals are considered to be part of the same trace. The iteration index within the evolution process and the fitness of all individuals taking part of a trace are stored.

We can think of three different types of traces questioning the following: *(1) Traces from the initial population:* Are substructures of the initial population still persistent in a later evolution stage? *(2) Backward traces from distinct fitness jumps:* Which trace is mainly responsible for the increase in performance, or which characteristic substructure is part of this best performing individual? *(3) Backward traces from the final population:* How many traces and which substructures constitute the final population?

Referring to the survivability of the initial population's substructures it is observed within our specific example [11], that, even when most of the patterns die out within the first 25% of the optimization process, there are still two traces that play a major role during the overall evolution. This shows that proper initialization – i.e., the initial population's quality of diversity – may have a considerable impact on the evolution's outcome. Different initialization schemes (e.g., using deterministic or heuristic number generators instead of standard pseudo-random processes) are now under extensive investigation.

The history of substructures which provoke distinct fitness jumps reveals the coexistence of different competing patterns within the evolving population. Some substructures will temporarily be at

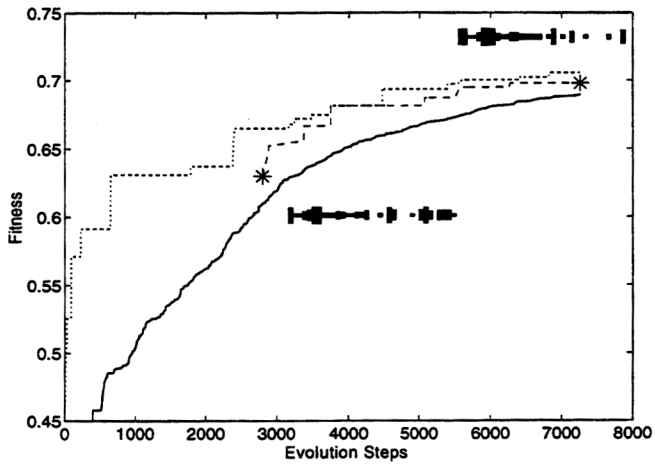

Fig.13: To observe if there are still different sub-populations in the actual or final population, a trace back to earlier stages of the population's evolution may be created. By doing so, it is possible to observe how the evolution of sub-populations takes place. Therefore the parallelism in the evolution is clearly visible. For these examples, the backward traces are shown for a population at 7300 evolution steps.

the top of the population's fitness ranking, while others are successful another time [11].

Considering the traces that constitute a final population (as depicted in *Fig.13*) this competition of patterns turned out to be a mean measure when qualifying an optimizer's potential termination state:

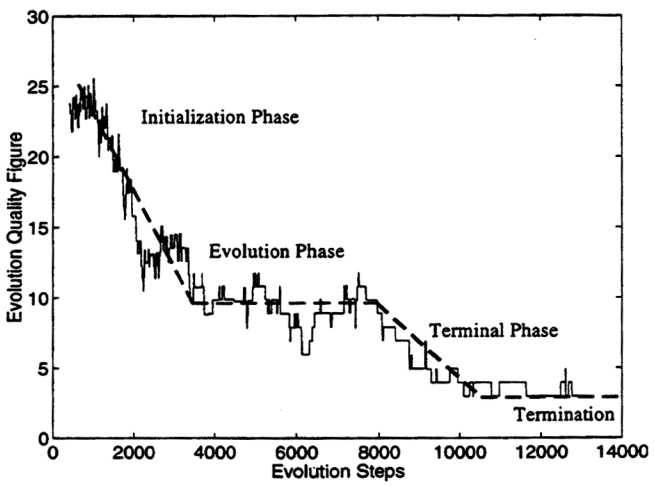

Fig.14: Value of the evolution figure during the optimization. Four phases may be distinguished where the labelling is proposed for visual purposes only.

qualifying an optimizer's potential termination state: Each substructure may be interpreted as a part of a sub-population of individuals containing this unique pattern, exemplifying as well that parallel optimization of different structures takes place even in a final evolution state. To dispose of different sub-populations at such stages underpins the impact of cross-over at the expense of mutation, indicating the optimization being still in an efficient operation mode compared to a purely statistically driven random search process. Thus, quantifying the *vitality* of a population after n iteration steps a *state variable* may be defined as follows [11]

$$C_P(n) = \frac{1}{F(n)} \sum_{i=1}^{N^{SP}(n)} F_i^{SP}(n)$$

where $F(n)$ stands for the temporal maximum fitness, N^{SP} represents the total number of sub-populations and $F_i^{SP}(n)$ assigns the maximum fitness within the i-th sub-population. *Fig14* shows the evolution of $C_p(n)$, whereas a categorization containing four different phases in the evolution process has been proposed. Here, $C_p(n)$ may be viewed as a specific representation of the number of competing patterns within the population involved.

7.3 EPILOGUE

We believe, when provided with both *structural* and *temporal* information of a population's evolution one should be able to define certain measures [8], [11] concerning, e.g., the vitality of the population or even a specification of its actual state of evolution. In order to underpin such ventured conjectures extensive statistical investigations are strictly inevitable, including also a much broader spectrum of examples than presented here. However, a lack of generality considering all attempts when formalizing the evolutionary algorithm's learning process will always remain. Therefore, other promising combinatorial optimization methods have to be compared when relying on an evolutionary paradigm. For the assessment of problem specific search space characteristics, hybridization of *evolutionary algorithms* with other methods should be investigated as well.

8. TOWARDS COMPUTER GUIDED ENGINEERING

Apart from the algorithmic considerations depicted in the previous Section 7 we will now briefly sketch two lines, where our research on evolutionary optimization in computational optics is about to advance. Within both strategies we always rely on the gathering of specific information regarding, e.g., the actual shape of the structure involved, the simulator's peculiarities and even the functional dependencies on the circuit level.

8.1 IMPROVEMENTS WITHIN ADVANCED DEVICE OPTIMIZATION PROBLEMS

At present we are strongly involved in the design of complex smart planar optical transducer elements for (bio-)chemical and physical sensor systems. Within these activities we believe we will obtain a deeper insight into the mechanisms of optical coupling and for the design of new grating couplers [35], especially of ultra-compact highly non-periodic coupler topologies. A rigorous design of such dense electromagnetic field coupling configurations usually represents an inverse scattering problem, which can only be solved with a combination of highly sophisticated codes for computational electromagnetics coupled to, e.g., an *evolutionary optimizer*.

When one links such optimization procedures with such simulation tools, one faces several difficult problems. As its main task the code for computational electromagnetics solves a so-called *forward problem* for the optimization procedure. Even when the time spent for the *forward problem* is long, the results have a limited accuracy. This may cause some noise within the data, which considerably disturbs the search process. Thus, the forward problem has to be solved many times. Referring to these issues, three different specifications should be respected when carefully looking for an appropriate forward solver: *1.)* The simulation program should be as *efficient* as possible, *2.)* it should maintain a *complete robustness* while possibly treating solutions not even thought to exist, and *3.)* it is mandatory that the solver delivers an *error measure* in order to guarantee a certain *accurateness* of the search process.

The *multiple multipole* (*MMP*) method [34] is a well-established, semi-analytical tool for solving time-harmonic 2D and 3D scattering problems within piecewise linear, homogeneous and isotropic domains. It is based on the *generalized multipole technique* (*GMT*). With *MMP*, the field f_D within individual domains D is approximated by a sum of N cylindrical or spherical multipole expansion functions f_{Dj}

$$f_D = f_{D0} + \sum_{j=1}^{N} A_{Dj} \cdot f_{Dj} + Error$$

which are themselves analytical solutions of the Helmholtz equation, where f_{D0} stands for the excitation.

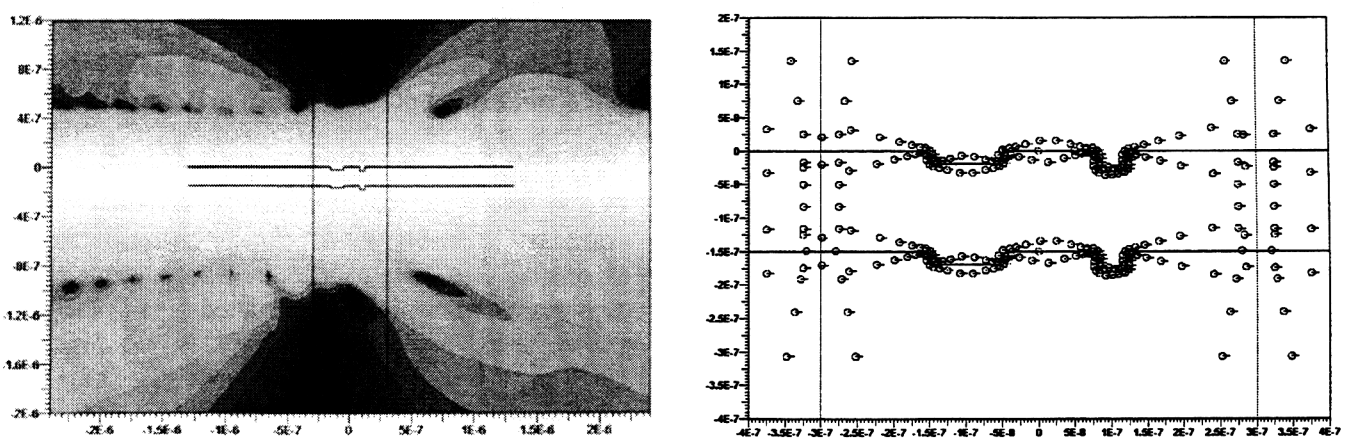

Fig.15: MMP calculation of a single slab waveguide perturbation pattern: (left) Intensity plot of the time-averaged Poynting field for TE-excitation from the left side. (right) Distribution of the corresponding multipole expansions (each multipole location is indicated by a small circle, boundaries are drawn as solid lines). The slab waveguide system consists of a TiO_2 core layer (thickness 150 nm), a H_20 upper cladding layer and polycarbonate as lower cladding respectively. The two grooves (1: width 100 nm, depth 20 nm; 2: width 40 nm, depth 30 nm) are separated by 200 nm. The operating wavelength is 785 nm (vacuum).

The origins for multipole expansions are usually set along the boundary of the domains in which the field is to be calculated. For the field around voluminous domains *Hankel*-type expansions are used whilst *Bessel*-type expansions are preferred inside. Other special functions are included as well, e.g., propagating and evanescent plane waves. The coefficients A_{Dj} are obtained by enforcing the boundary conditions for the field components at discrete matching points on the boundary. Since more matching points are introduced than necessary, the *MMP* method leads to an overdetermined system of equations. This system is solved in the least-square sense which is equivalent to an error minimization technique. Thus, an adequate *error measure* is inherently delivered by the method itself.

In order to maintain *robustness* during an optimization scenario, *MMP* should be insensitive to all parameter variations involved. Here, the most challenging task is to successfully adapt the simulation to repeated changes of the coupler's grating shape. For that reason we have developed a fully automatic pole-setting procedure which allocates all multipole expansions needed along their corresponding boundaries. The proper setting takes into account several properties of the actual shape as well as it considers implicit portions such as, e.g., the curvature and its context within the boundary's devolution. The *MMP* calculation shown in *Fig.15* is fully based on the automatic pole distribution procedure and it concerns a preliminary perturbation pattern which may constitute a grating coupler within our typical sensor configuration.

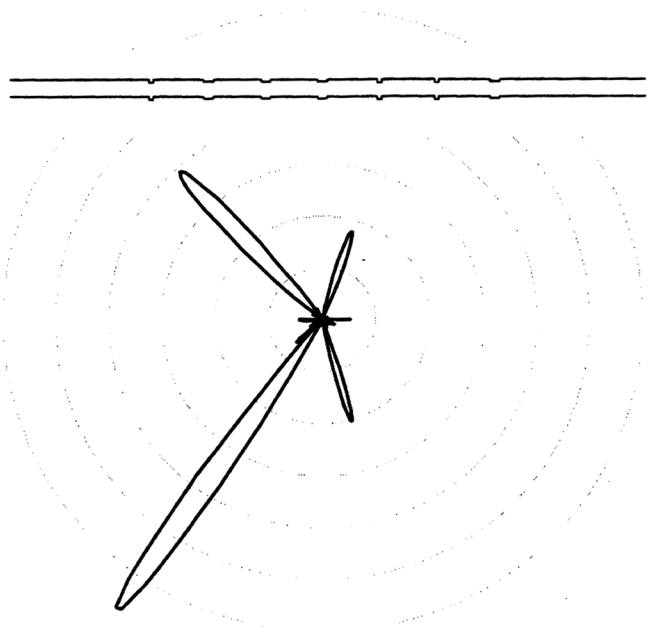

Fig.16: Non-periodic grating: Polar plot of the radiated far-field (time-averaged Poynting field) for TE-excitation from the left side. The inset shows the 7 fold concatenation of various single perturbations as described in Fig.15.

Besides the semi-analytical nature of *MMP*, there are further algorithmic potentialities when improving the program's *efficiency*. The *parameter estimation technique* (*PET*) is a very powerful technique that can be applied to numerical codes based on dense matrices as a power booster for the computation of the response of electromagnetical or optical problems at, e.g., different frequencies. It is applied to the *multiple multipole* (*MMP*) method in conjunction with the method of *conjugate gradients* (*CG*) for iteratively and efficiently solving the rectangular *MMP* matrix. The general idea of the *parameter estimation technique* (*PET*) is the evolutionary recycling of knowledge. Since all the expansion parameters $A_{Dj}^{(k)}$ (and functions f_{Dj}) are usually known from previous $1 \ldots k$ runs while, e.g., sweeping the wavelength λ, recycling of knowledge means nothing else but a pertinent extrapolation technique for estimating the parameters $A_{Dj}^{(k+1)}$ to be computed in the current run k. This speedup technique has already been detailed in earlier contributions to *ACES* publications [15], [16].

The most powerful mean to economize computational effort can be achieved, when focusing solely to characteristic portions of the overall coupler structure. Hence, we have developed a *near-to-far-field transformation* which allows the radiation field of a waveguide perturbation being approximated simply by a single particular multipole expansion. Each partial perturbation pattern can be analyzed within minutes and is then at the optimizer's disposal. Having available a library of such generic far-field expansions, the radiation field of the overall coupler topology is immediately calculated when placing the particular expansions accordingly. *Fig.16* depicts the far-field of a grating structure consisting of a seven fold concatenation of the perturbation analyzed in *Fig.15*. Within the scope of a realistic optimization scenario, the scalability due to the problem's complexity may be less severe, inasmuch a speedup of around two orders of magnitudes has become achievable. Constituting the field solution of highly-non-periodic grating structures as to the same degree of simplicity like in periodic ones (treating the

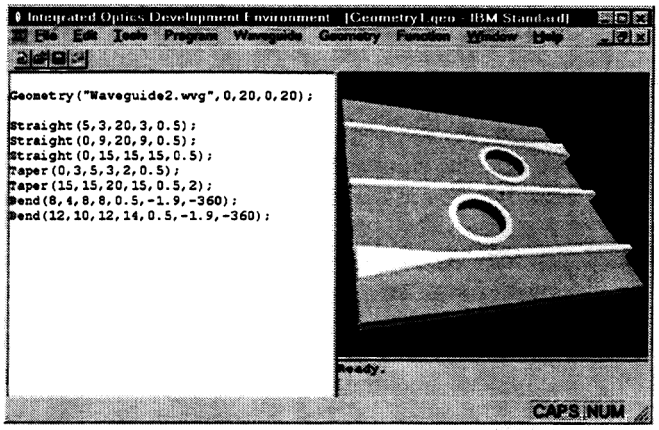

Fig.17: User interface of the developed design platform. (left) Formal description of the waveguide elements. (right) View of the corresponding planar integrated optical circuit topology.

grating's unit-cell with periodic boundary conditions) [36] reveals an unique attractiveness especially when targeting irregular topologies. This allows us to face novel design scenarios leading probably to unexpected topological coherence and implying readjusted representation schemes.

8.2 MOVING TOWARDS THE CIRCUIT LEVEL

On the system level, we are facing yet one of the most demanding *inverse problems:* designing an entire integrated optical circuit based solely on optical specifications. Resting on the expertise of the optimization examples presented earlier, our research is now focused to the development of a design platform for planar integrated optics devices. This

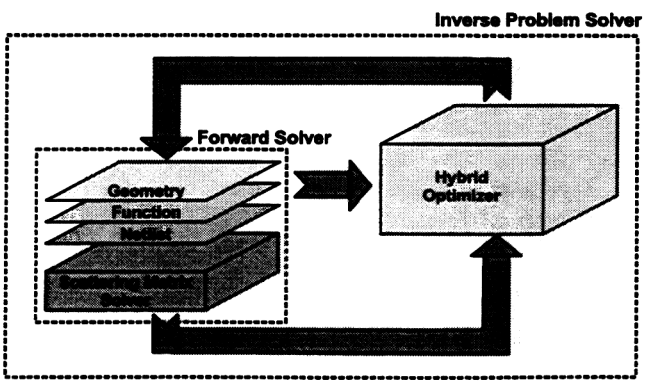

Fig.18: General architecture of the developed design and optimization platform.

design environment whose user interface is imaged in *Fig.17* relies on sophisticated representation schemes for device *geometries* based on elementary waveguide structures (e.g., straight waveguides, bends and tapers). While performing a *semantic analysis* the program is able to identify the potential *functionality* of a combination of such elements leading to "auto generated" optical circuits including, e.g., directional couplers and splitters of different shapes. For a rapid evaluation of each device topology under optimization a fast *scattering-matrix* approach is primarily used. *Fig.18* shows the general architecture of our optimization platform where the forward solver is allocated by the hierarchical representation scheme of the underlying problem.

As an optimizer we consider a kind of *evolutionary strategy* (*ES*) scheme. In order to formalize the optimizer's interference during optimization several *interference operators* have been designed. Looking for appropriate schemes on how to distort a circuit geometry or how to accordingly modify an element's functionality represents the most demanding part of our implementation. Besides translational and rotational distortion of the circuit while maintaining connectivity other operators such as scaling, and the introduction of predefined functional building blocks are under extensive investigation.

Some simple preliminary test cases like, e.g., the optimization of a multi-stage resonant-coupler add-drop device have clearly shown that the optimization problem posed here reveals an enormous search space. Even when assessing a 2D circuit topology to its inherent functionality has major influence on the problem's complexity, we still rely on our approach: Including semantic information like the circuit's intrinsic interrelations within an optimization process seems the only way to keep the problem tractable. Nevertheless, we believe our evolutionary design environment [37] to be very flexible because it does not necessarily require a preliminary design as a starting configuration and even allows modifications of the problem representation during the optimization process itself.

9. CONCLUSION

By means of five design examples we have demonstrated why *evolutionary algorithms* are highly qualified to solve "real world" inverse problems considering various applications in the field of planar

integrated optics, optical communication technology, and dielectric material modeling as well. The modal treatment of optical fields by an appropriate underlying structure is an essential operation regarding the characteristic functionality of the resulting device. Therefore, we have presented examples related to both the *spectral* shaping of the optical field (single mode multi-cavity laser diodes and concatenated Bragg grating filters) and the *spatial* molding of the light (spot-size converter).

Leaving the field of *structural optimization* we focused then on two examples stemming both from an applied engineering background.

First, a purely *combinatorial* optimization problem solution has been drawn when improving the performance of modern optical communication systems (e.g., fiber optic SCM-links and high-speed WDM-systems) according to a more adapted frequency (or wavelength) carrier distribution. In the second example we report the *evolutionary algorithm's* parameter estimation feature on the determination of the dispersive properties of highly lossy, very complex dielectric materials starting from scattering parameter measurements.

After illustrating the various examples, the focus of this paper has changed towards a more prospective view where the *evolutionary algorithm's* ability to gather problem-related information during optimization is addressed. Here, we propose to benefit from *structural* interdependencies within a population of potential solutions as well as to trace different *temporal* evolution aspects in order to establish corresponding superior meta-optimization strategies.

One obvious area for future research on *evolutionary optimization* has already been annotated by the improvement of the *forward solver* with respect to speedup, robustness and accuracy. Moving then to the circuit level we tried to use the optimizer as a proper design tool for planar integrated optics devices. Here, we have faced one of the most demanding inverse problems. It seems only tractable when including the circuit's intrinsic interrelations (by a *semantic analysis*) within the problem representation as well as implementing the optimizer's interference operators accordingly. Hence, extensive investigations are still mandatory. Nevertheless, we propose *evolutionary algorithms* being highly valuable candidates when evaluating codes for computer *guided* engineering and virtual design platforms.

10. REFERENCES

[1] On terminology: We call our *genetic algorithm* (*GA*) based optimization scheme *evolutionary algorithm* (*EA*) because of its *non-binary* genotype representation. Instead of the classical *GA's* binary chromosome we use *integer strings* in our *EA* implementation. Furthermore, the classical *GA* is a *generation based* scheme, where successful features are presumably transferred to a sequential part of the underlying population (the next generation) whereas our *EA* scheme rely on a *breeder type* [4] of optimization where only two off-springs are generated and reintroduced into the population replacing the worst two individuals. This latter optimization process is usually attributed to a *steady state GA* scheme.

[2] D. Erni, D. Wiesmann, M. M. Spühler, S. Hunziker, B. Oswald, J. Fröhlich and Ch. Hafner, *Recent Research Developments in Optical Engineering, Research Signpost, chapter* "Evolutionary optimization algorithms in computational optics," Recent Research Developments Series, Publisher: Research Signpost, Trivandrum, India,1999, still in press.

[3] D. Erni, J. Föhlich, and O. J. Homan, "Analysis and optimization of non-periodic coupled-cavity laser diodes," *Latsis Symposium on Computational Electromagnetics*, 19-21, Zürich, Switzerland, pp. 248-254, Sept. 1995.

[4] H. Mühlenbein, D. Schlierkamp-Voosen, "Predictive models for the breeder genetic algorithm," *Evolutionary Computation*, vol. 1, no. 1 pp. 25-49, Spring 1993.

[5] D. Erni, *Periodische und nichtperiodische Wellenleitergitter- und Laserkavitätskonzepte*. Diss. ETH, No. 11654, Zürich, 1996.

[6] J. Fröhlich, *Evolutionary Optimization for Computational Electromagnetics*. Diss. ETH, No. 12232, Zürich, 1997.

[7] D. Erni, "Nichtperiodische Konzepte in integrierten optischen Wellenleiterstrukturen," *Bulletin SEV/VSE 3/97*, vol. 88, no. 3, pp. 11-16, März 1997.

[8] D. Erni, M. M. Spühler, and J. Fröhlich, "Evolutionary optimization of non-periodic coupled-cavity semiconductor laser diodes," *Optical and Quantum Electronics (OQE), Special Issue: The 1997 International Workshop on Optical Waveguide Theory and Numerical Modelling*, vol. 30, no. 5/6, pp. 287-303, May 1998.

[9] D. Erni, M. M. Spühler, and J. Fröhlich, "A generalized evolutionary optimization procedure applied to waveguide mode treatment in non-periodic optical structures," *8th European Conf. on Integrated Optics ECIO'97*, April 2-4, pp. 218-221, Stockholm, Sweden, 1997.

[10] M. M. Spühler, D. Erni, and J. Fröhlich, "Topological investigations on evolutionary optimized non- periodic optical structures," *1997 International Workshop on Optical Waveguide Theory and Numerical Modelling*, Sept. 19-20, University of Twente, the Netherlands, 1997.

[11] M. M. Spühler, D. Erni and J. Fröhlich, "An evolutionary optimization procedure applied to the synthesis of integrated spot-size converters," *Optical and Quantum Electronics (OQE), Special Issue: The 1997 International Workshop on Optical Waveguide Theory and Numerical Modelling*, vol. 30, no. 5/6, pp. 305-321, May 1998.

[12] M. M. Spühler, B. J. Offrein, G.-L. Bona, R. Germann, I. Massarek and D. Erni, "A very short planar silica spot-size converter using a non-periodic segmented waveguide," *J. Lightwave Technol.*, vol. 16, no. 9, pp. 1680-1685, Sept. 1998.

[13] M. M. Spühler, B. J. Offrein, G.-L. Bona, R. Germann, and D. Erni, "Compact spot-size converter using non-periodic segments for high refractive index contrast planar waveguides," *European Conference on Lasers and Electro-Optics CLEO'98* Sept 13.-18., Glasgow, UK., CWN3, pp. 234, 1998.

[14] D. Wiesmann, D. Erni, J. Fröhlich, H. Rothuizen, R. Germann, G.-L. Bona, Ch. David and H. Jäckel, "Apodization of a grating filter by concatenation of Bragg gratings with different ridge patterns," *9th European Conf. on Integrated Optics ECIO'99*, April 14-16, Torino, Italy, WeG, pp. 159-162, 1999.

[15] Ch. Hafner, "MMP-CG-PET: The parameter estimation technique applied to the MMP code with the method of conjugate gradients," *ACES Journal.* vol. 9, no. 3, pp. 28-38, 1994.

[16] Ch. Hafner, J. Fröhlich, "The parameter estimation technique (PET): Speeding up dense matrix methods," *Proceedings of the 11th Annual Review of the Applied Computational Electromagnetic Society*, Monterey, CA, 1995.

[17] S. Hunziker, *Analyse und Optimierung faseroptischer SCM-Links*. Diss. ETH, No. 12604, Zürich, 1998.

[18] B. Oswald, D. Erni, H. R. Benedickter and W. Bächtold, "Dielectric properties of natural materials," *IEEE-AP Soc. Int. Symp., Conf. on Antennas and Propagation*, Atlanta, pp. 2002-2005, June 22-26, 1998.

[19] G. Björk, O. Nilsson, "A new exact and efficient numerical matrix theory of complicated laser structures: properties of asymmetric phase-shifted DFB lasers," *J. Lightwave Technol.*, vol. 5, no. 1, pp. 140-146, Jan. 1987.

[20] D. Wiesmann, J. Hübner, R. Germann, I. Massarek, H. W. M. Salemink, G.-L. Bona, M. Kristensen and H. Jäckel, "Large UV-induced negative index changes in germanium-free nitrogen-doped planar SiO_2 waveguides," *IEE Electron. Lett.*, vol. 34, no. 4, pp. 364-365, Feb. 1998.

[21] J. Hübner, D. Wiesmann, R. Germann, I. Massarek, B. J. Offrein, and M. Kristensen, "Strong Bragg gratings induced with 248 nm light in buried silicon oxynitride waveguides," *OSA Topical Meeting on Bragg Gratings, Photosensitivity, and Poling Glass Fibers and Waveguides: Applications and Fundamentals.* Williamsburg, VA, Oct. 26-28, 1997.

[22] H. Sakata, "Sidelobe suppression in grating-assisted wavelength-selective couplers," *Opt. Lett.*, vol. 17, no. 7, pp. 463-465-2043. April 1992.

[23] T. A. Strasser, P. J. Chandonnet, J. DeMarco, C. E. Soccolich, J. R. Pedrazzani, D. J. DiGiovanni, M. J. Andrejco, and D. S. Shenk, "UV-induced fiber grating OADM device for efficient bandwidth utilization," *Proc. Opt. Fiber. Commun. Conf., OFC'96*, vol. 2, Feb. 25 – March 1, San José, CA, USA, pp. 360-363, 1996.

[24] N. Matuschek, F. X. Kärntner, U. Keller, "Exact coupled-mode theories for multilayer interference coatings with arbitrary strong index," *IEEE J. Quantum Electron.*, vol. 33, no. 3, pp. 295-302, March 1997.

[25] J. A. Dobrowolski, "Numerical methods for optical thin films," *OSA Optics & Photonics News*, pp. 25-33, June 1997.

[26] K. De Mesel, I. Moerman, R. Baets, B. Dhoedt, P. Van Daele, and Jiri Stulemeijer, "Spot size converters for low cost PICs," *9th European Conf. on Integrated Optics ECIO'99*, April 14-16, Torino, Italy, ThC, pp. 253-258, 1999.

[27] S. Jüngling, J. C. Chen, "A study and optimization of eigenmode calculations using the imaginary-distance beam-propagation method," *IEEE J. Quantum Electron*, vol. 30, no. 9, pp. 2098-2105, Sept. 1994.

[28] S. Hunziker and W. Bächtold, "Cellular remote antenna feeding: optical fibre or coaxial cable?" *IEE Electron. Lett.*, vol. 34, no. 11, pp. 1038-1040, 28th May 1998.

[29] S. Hunziker and W. Bächtold, "Fiber dispersion induced nonlinearity in fiber-optic links with multimode laser diodes," *IEEE Photon. Technol. Lett.*, vol. 9, no. 3, pp. 371-373. March 1997.

[30] S. Hunziker, "Volterra analysis of second- and third-order intermodulation of InGaAsP/InP laser diodes: theory and experiment," *Opt. Eng.*, vol. 34, no. 7, pp. 2037-2043. July 1995.

[31] S. Hunziker and W. Bächtold, "Simple model for fundamental intermodulation analysis of RF amplifiers and links," *IEE Electron. Lett.*, vol. 32, no. 19, pp. 1826-1827. Sept. 1996.

[32] R. W. Tkach, A. R. Chraplyvy, F. Forghieri, A. H. Gnauck, R. M. Derosier, "Four-photon mixing and high-speed WDM systems," *J. Lightwave Technol.*, vol. 13, no. 5, pp. 841-849, May 1995.

[33] P. Sheng, *Introduction to Wave Scattering, Localization, and Mesoscopic Phenomena.* San Diego: Academic Press, 1995.

[34] Ch. Hafner, *Post-modern Electromagnetics – Using Intelligent Maxwell Solvers.* Chichester, West Sussex, UK: John Wiley & Sons, 1999.

[35] D. Erni, "MMP analysis of very short doubly perturbend waveguide structures," *7th European Conf. on Integrated Optics ECIO'95*, April 3-6, Delft, The Netherlands, pp. 387-390, 1995.

[36] Ch. Hafner, "Efficient MMP computation of periodic structures ," *Proceedings of the 10th Annual Review of the Applied Computational Electromagnetic Society*, March 21-26, pp. 303-310, 1994.

[37] M. M. Spühler, D. Erni, "Structural optimization in planar integrated optics," *1999 International Workshop on Optical Waveguide Theory and Numerical Modelling,* Sept. 23-25, The University Jean Monnet, Saint-Etienne, France, 1999.